CRREL
REPORT 76-10

De-icing using lasers

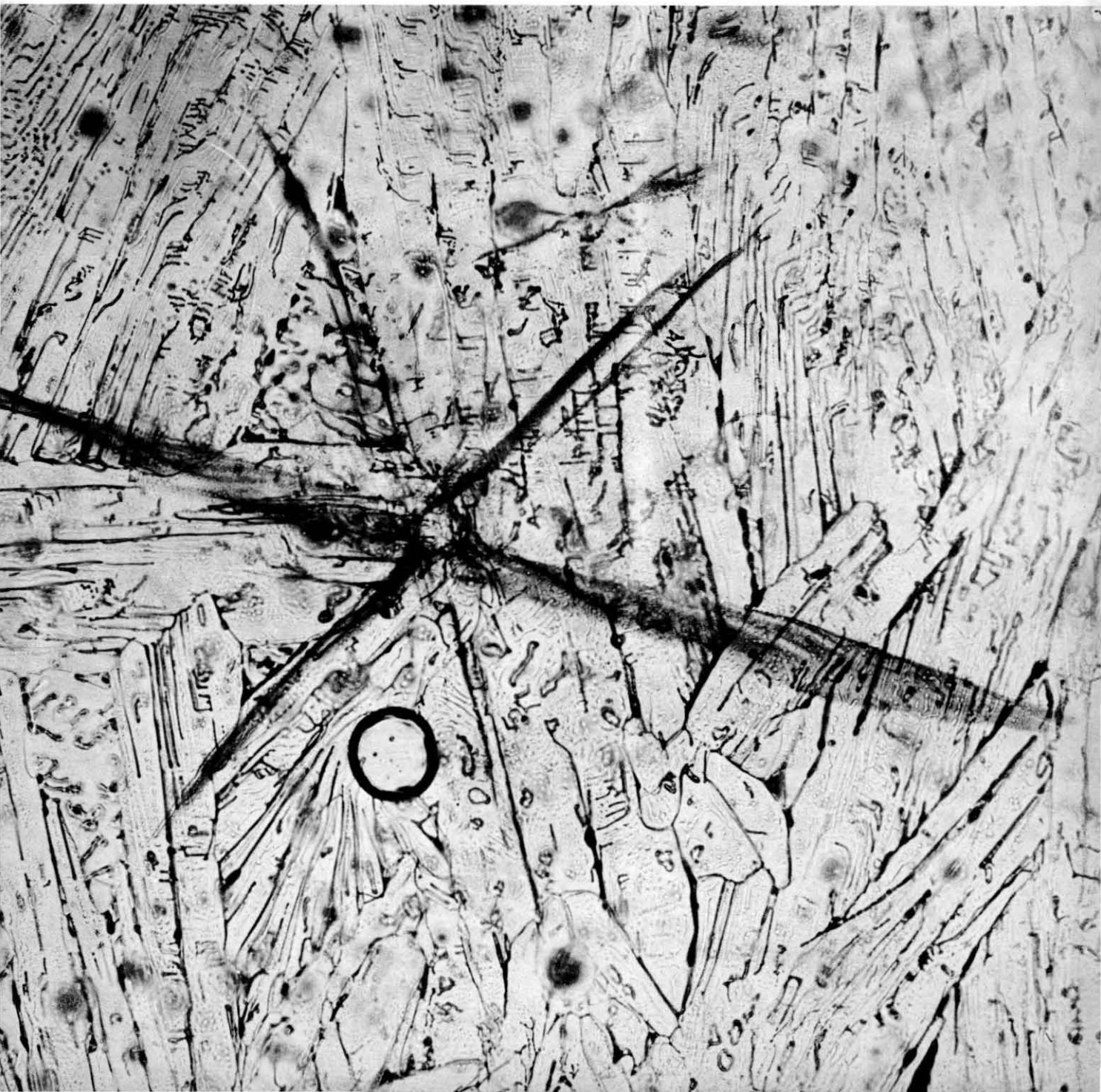

Cover: Typical six-sided crack produced in single-crystal ice on glass substrate by 6-megawatt Nd:Glass laser beam. (Photograph by Stephen J. Marshall.)

CRREL Report 76-10

De-icing using lasers

Jean W. Lane and Stephen J. Marshall

April 1976

Prepared for
U.S. ARMY MATERIEL COMMAND
By
CORPS OF ENGINEERS, U.S. ARMY
COLD REGIONS RESEARCH AND ENGINEERING LABORATORY
HANOVER, NEW HAMPSHIRE

The findings in this report are not to be construed as an official Department of the Army position unless so designated by other authorized documents.

REPORT DOCUMENTATION PAGE

READ INSTRUCTIONS BEFORE COMPLETING FORM

1. REPORT NUMBER: CRREL Report 76-10
2. GOVT ACCESSION NO.:
3. RECIPIENT'S CATALOG NUMBER:
4. TITLE (and Subtitle): DE-ICING USING LASERS
5. TYPE OF REPORT & PERIOD COVERED:
6. PERFORMING ORG. REPORT NUMBER:
7. AUTHOR(s): Jean W. Lane and Stephen J. Marshall
8. CONTRACT OR GRANT NUMBER(s):
9. PERFORMING ORGANIZATION NAME AND ADDRESS: U.S. Army Cold Regions Research and Engineering Laboratory, Hanover, New Hampshire
10. PROGRAM ELEMENT, PROJECT, TASK AREA & WORK UNIT NUMBERS: DA Project IT161102B52A, Task 02, Work Unit 008
11. CONTROLLING OFFICE NAME AND ADDRESS: U.S. Army Materiel Command, Washington, D.C.
12. REPORT DATE: April 1976
13. NUMBER OF PAGES: 30
14. MONITORING AGENCY NAME & ADDRESS (if different from Controlling Office):
15. SECURITY CLASS. (of this report): Unclassified
15a. DECLASSIFICATION/DOWNGRADING SCHEDULE:
16. DISTRIBUTION STATEMENT (of this Report): Approved for public release; distribution unlimited.
17. DISTRIBUTION STATEMENT (of the abstract entered in Block 20, if different from Report):
18. SUPPLEMENTARY NOTES:
19. KEY WORDS (Continue on reverse side if necessary and identify by block number):

Control	Interactions	Test methods
Damage	Lasers	Tools
Deicing systems	Materials	
Failure	Reaction kinetics	
Ice	Targets	

20. ABSTRACT (Continue on reverse side if necessary and identify by block number)

The feasibility of employing a laser to de-ice remote surfaces was investigated. A Nd:Glass laser, wavelength 1.06 micrometers, and a Ruby laser, wavelength 6943 Å, were used to irradiate ice grown upon six types of substrates – asphalt, brass, concrete, aluminum, steel, and stone. It was found that a single pulse, delivered to the interface between the ice and its substrate at a power density of 10^8 to 10^9 watts/cm^2, produced fractures 0.1 to 2 cm in diameter for all substrates. If the initial fracture could be propagated by suitable scanning of the optical beam over the interface, the ice could be disrupted and thus removed from the substrate. The technique could also be a useful adjunct to de-icing methods that depend upon the existence of an initial crack. The process of producing the initial

fracture was found to be limited by the thickness of the ice, the bubble content of the ice, and the focusing system.

PREFACE

This report was prepared by Captain Jean W. Lane, R&D Coordinator, and Stephen J. Marshall, Physical Science Technician, of the Physical Sciences Branch, Research Division, U.S. Army Cold Regions Research and Engineering Laboratory. The work was done under DA Project 1T161102B52A, *Mobility and Environmental Research*, Task 02, *Military Aspects of Cold Regions Research*, Work Unit 008, *Adhesion and Physics of Ice*. Initial efforts of this study were performed as part of the In-house Laboratory Initiated Research (ILIR) program.

Technical review of the report was performed by Dr. Kazuhiko Itagaki and Dr. Richard Munis of CRREL. The authors gratefully acknowledge the help rendered by Roger H. Berger throughout the project.

CONTENTS

Figure

TABLES

SUMMARY

It was found that a pulsed laser of ordinary commercial design could be used to fracture ice of thicknesses less than 2 cm if the optical beam could be focused on the interface of the ice and the structure to be de-iced. It was shown that inexpensive simple convex lenses are sufficient for a focusing system but that a practical de-icing system would require the design of a mounting system that would be capable of adjusting the position of the focal point so that it would scan the surface to be de-iced at a rate commensurate with the degree of fracture propagation needed to remove ice or prevent its accretion.

Advances in design have made the helicopter a key element in tactics requiring exceptional mobility. Consequently, the need for helicopters to be operable in all types of weather has become acute. This study tested the feasibility of using a laser to combat icing problems (such as those of a helicopter's rotor blade) not amenable to conventional methods. A laser system already used for target acquisition and analysis or navigation might be redesigned to include a de-icing capability. A single system would be made to do the work of two without additional weight and space consumption.

DE-ICING USING LASERS

Jean W. Lane and Stephen J. Marshall

INTRODUCTION

It has been demonstrated[20 23] that intense monochromatic optical beams can interact strongly with materials that, at lower energies, are transparent to light of optical frequencies. Ice is a transparent material at optical frequencies and low energies.[10] Are optical beams of sufficiently high energies capable of damaging ice? The commercial production of lasers has opened this possibility to study.

Optical damage to normally transparent materials such as quartz has been observed to consist largely of cracks, both on the surface and in the bulk,[3 7] so this is the type of optical damage to expect in ice. The currently accepted mechanism for fracture specifies the initiation of microcracks, i.e. the "Griffith cracks," as a prerequisite for a material to fracture at a stress lower than its theoretical elastic limit.[12 25] A laser could initiate microcracks in ice and induce it to fracture at low stress.[27] This could be used to aid in the removal of ice from surfaces where icing is a problem. It is the purpose of this work to investigate this possibility.[17]

EXPERIMENTAL WORK

Study of literature on the environmental conditions that produce icing[1] led to the selection of -20°C as the ambient temperature at which to prepare and irradiate samples.

Several types of samples were studied in an effort to determine which aspects of a sample's physical state affected its interaction with the optical beam. Natural accretions of ice contain air bubbles, impurities, mechanical deformations, and internal stresses. The surface of such ice is irregular, and, in general, the bulk is polycrystalline. The substrate upon which the ice forms may affect the growth of the accretion and interact with the optical beam. This implies that any comprehensive list of parameters relevant to optical study of ice adhering to a substrate must include surface structure of the ice and the substrate, thickness of ice parallel to the optical beam, concentrations of impurities and air bubbles in the ice, crystallographic orientation, grain sizes, and type of substrate. (In this work, unless otherwise indicated, "thickness" will refer to the dimension of a sample that is parallel to the optical beam and will measure only the ice.) These experiments were limited to consideration of surface structure of the ice, thickness, crystallographic orientation of the ice, and type of substrate. Each type of sample is identified and described below.

SCR samples

The first type of sample was a single crystal that had been cut from the Mendenhall Glacier. The crystallographic orientation of these samples was determined by a technique that has been

a. Separate components – mold, substrates, and gasket assembly. The fourth hole in the mold was intended to provide unobstructed passage of the optical beam when the mold with samples was inserted into the optical system. Removal of the samples proved to be more feasible so this feature was never used.

b. TRICIA assembled except for top gasket and ready for filling.

Figure 1. TRICIA (the rubber, insulated, confined ice apparatus).

developed by Itagaki.[13] Each sample was mounted upon a glass slide; the average thickness was 1 cm. The surface of each sample was rendered optically flat (by a technique due to Tobin and Itagaki[26]) immediately before insertion in the optical system. There were no visible bubbles or impurities. Samples prepared in this manner will be called SCR (for "single-crystal") samples.

CAG samples

The second type of sample was a polycrystal prepared from distilled water in the following manner. A cylindrical mold of Dow Corning Silastic, an RTV moldmaking rubber, to be hereafter known as TRICIA (for "the rubber, insulated, confined ice apparatus"), was used (Fig. 1). TRICIA contained three cylindrical holes, each of which was fitted with a removable, snugly fitting 5-mm-thick disc of a material selected as substrate. These discs were made of three different materials – aluminum, brass and steel. The holes were 1, 2 and 3 in. (2.5, 5 and 7.5 cm) in diameter. TRICIA was sealed on each face by rubber gaskets. With the bottom sealed and the substrates pressed firmly against the gasket, water was poured into each hole, and the top sealed with a rubber gasket under the pressure of lead weights. After freezing, the gaskets were removed and the samples pressed from the holes. Since the flexible walls and gaskets of TRICIA allowed expansion pressures and surface tension to be relieved during freezing, the samples were strain-free and smooth-surfaced

Figure 2. Preparation of UAG samples. The six identical plastic containers are shown with the six samples that were prepared. The black markers on the containers indicate depth of filling. The six substrates – aluminum, steel, brass, asphalt, concrete, and porous stone – are frozen into the bottom of the samples.

relative to any natural accretion of ice upon the same substrate. Thicknesses of 1, 2 or 3 in. (2.5, 5 or 7.5 cm) were available with this method of preparation. There were no visible impurities but the center of the ice was rendered translucent by visible bubbles. Samples of this type will be called CAG (for "confined-as-grown") samples.

CMS samples

The third type of sample was a polycrystal prepared from distilled water in the same manner as the CAG samples. Immediately before insertion into the optical system, the surfaces of these samples were further smoothed by use of a microtome with a steel blade. Samples of this type will be called CMS (for "confined microtomed surface") samples.

UAG samples

The fourth type of sample was prepared from distilled water by use of flexible plastic containers, the 3-in.-diam (7.5-cm-diam) discs used with TRICIA, and three additional discs of the same thickness as those used for TRICIA but varying in diameter and material (Fig. 2). The additional discs were concrete of 3-in. (7.5-cm) diam, asphalt of 5.3-cm diam, and porous stone of 6.4-cm diam. The plastic containers were rectangular pint-sized containers produced commercially for the storage of food. The six substrates were placed on the bottoms of six containers. Water was added to cover the substrates to depths of 0.5, 1.0, 1.5, 2.0 or 3.0 cm and this depth was taken as the thickness of the resulting samples. No constraint was placed upon the water's surface during freezing. After freezing, the samples were removed by flexing the containers. As the water was unconfined on one surface during freezing, surface tension and expansion pressures caused the central region of the surface to rise into a cracked hump. Differential rates of thermal contraction for ice and substrate caused other large fissures and cracks to extend through the bulk of the sample. The size of the container's cross section was selected and the substrate positioned so as to make the samples fit into the optical system with the undamaged portions of ice aligned in the beam. The thickness of these portions was within a millimeter of the original depth of filling. There were no visible impurities. Visible bubbles were evenly distributed throughout most of the volume, rendering all of the ice (except the region immediately adjacent to the interface with the substrate) translucent. This type of sample will be called UAG (for "unconfined-as-grown") samples.

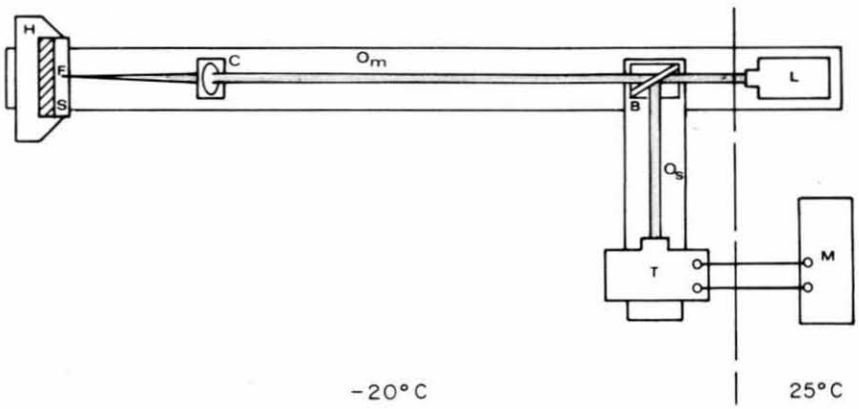

Figure 3. Schematic diagram of the optical system. Laser L, beam splitter B, ballistic thermopile T, main optical bench O_m, secondary optical bench O_s, converging lens C, focal spot F, sample S, holder H, energy meter M. The dashed line indicates which components were at room temperature and which at -20°C.

SI samples

The fifth type of sample was prepared from sea water collected from the coast of Maine in August 1973. The salinity of the sea water was measured as 29 g/kg. With the exception of the type of water, these samples were prepared exactly like CAG samples. These samples appeared uniformly translucent, very nearly opaque. This type of sample will be called SI (for "sea ice") samples.

Optical system

The configuration of the optical system is shown in Figure 3. The laser L produced a monochromatic pulse of light. This pulse impinged upon a beam splitter B, which diverted 10% of the intensity into a ballistic thermopile T (mounted on the secondary optical bench O_s) and allowed 90% of the intensity to continue parallel to the main optical bench O_m to a converging lens C which focused the light so that the focal spot F fell upon the sample S (mounted in the holder H) in one of three positions – surface, center of the bulk, or interface between ice and substrate. The output of T was sent to the energy meter M. Light-absorbent paper, placed at F with the sample removed, allowed the diameter d of F to be measured. The energy density W of the pulse at F could then be calculated from d and the reading ϵ of M by use of

$$W = 36\epsilon/\pi d^2 . \qquad (1)$$

The dashed line dividing the components in Figure 3 indicates that all of the components except L and M were maintained at the temperature of -20°C at which the samples were prepared and stored.

Equipment

The laser was a Hadron/TRG Model 104A laser system with interchangeable rods, one of ruby and the other of Nd:Glass. A Hadron/TRG Model 104A-3 rotating prism Q-switch allowed the laser two modes m of operation. For the normal mode of operation ($m = N$) the Q-switch was disengaged and the pulse-width was 0.8 to 2 milliseconds. For the Q-switched mode of operation ($m = Q$), the

Q-switch was engaged and the pulse-width was 30 to 50 nanoseconds. A Hadron/TRG Model 0104A-1 laser power supply provided power to the laser and a means to vary the energy in a given pulse by variation of the input to the laser. When the ruby rod was used, the laser produced pulses of 6 joules (maximum) for $m = N$ and 1 joule (maximum) for $m = Q$ at a wavelength of 6943Å. With Nd:Glass, the laser produced pulses of 5 joules (maximum) for $m = N$ and 0.9 joule (maximum) for $m = Q$ at a wavelength of 1.06 micrometers.

The ballistic thermopile was a Hadron/TRG Model 101. The energy meter was a Hadron/TRG Model 102C. The main optical bench was a Hadron/TRG Model 120A precision laser bench, which was modified to use Oriel Model B-23-62 and Oriel Model B-23-52 carriers. The secondary optical bench was fabricated to attach to the main optical bench at right angles and to use the Oriel carriers. Salinity measurements were made with an Industrial Instruments Model RB2 Solu Bridge.

The lenses were of two types. The first, obtained from Edmund Scientific Company, was an inexpensive biconvex lens with 2.4-cm diameter. Focal lengths were 1.5, 3.5, 5.8, 6.4, 7.4, 10.2 and 18.1 cm. The second type was an Ealing glass biconvex lens with 1.52 index of refraction and 2.5-cm diameter. Focal lengths were 10, 15, 20, 25, 30 and 50 cm.

Procedure

An individual experimental run lasted two hours and was designed to acquire a specific type of information. Therefore, all runs were not conducted identically. Generally, a run began with checks on the position and alignment of the lens. This was followed by a determination of d. The sample was inserted into the optical system and the laser operated in the modes and at the settings of the power supply dictated by the objectives of the run. The sample was examined for damage after each pulse or series of pulses and the reading of the energy meter was recorded for each pulse. When the required irradiations had been completed, the sample was removed from the optical system and, if damage had been produced, an attempt was made to photograph this damage. Once all work on the sample had been completed, it was placed on a shelf in the same environment in which it had been prepared and studied until its substrate was needed to prepare new samples. Used samples were melted. The substrates were then dried, degreased with acetone, examined for any damage due to irradiation, and reused. Until needed in the optical system, samples were kept in protective coverings to retard sublimation. Except for SCR samples, the time that elapsed from the beginning of freezing to insertion in the optical system was recorded and called the "age" of the sample. In general, many samples were used in a run so that a specific sample did not remain in the optical system for more than 15 minutes.

PHOTOGRAPHIC WORK

The damage to be photographed varied in size from pits of the order of millimeters in diameter to fissures of the order of a few centimeters long. In addition, the damage displayed a variation of shapes dependent upon the point from which it was viewed so that a single photograph could not record the three-dimensional shape of the structure. Cracks and pits that were localized at the interface or in the bulk of the sample could not be photographed without some alteration of the sample, and any alteration of the sample risked the introduction of artifacts or the destruction of the sample. It was therefore necessary to use several methods of photographing damage. These methods, and the type of damage for which they were used, are described below. For more details, consult the work of Marshall.[18]

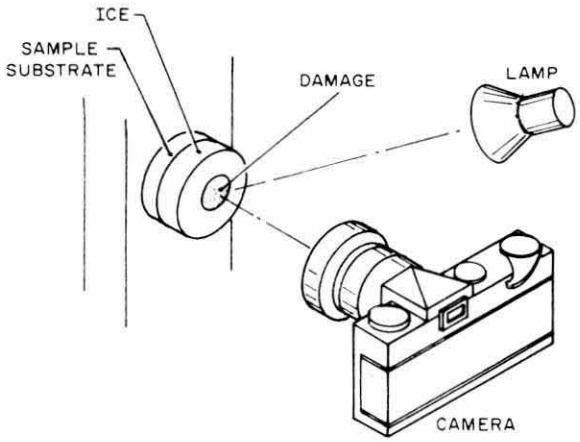

Figure 4. Photographic system for large-scale damage.

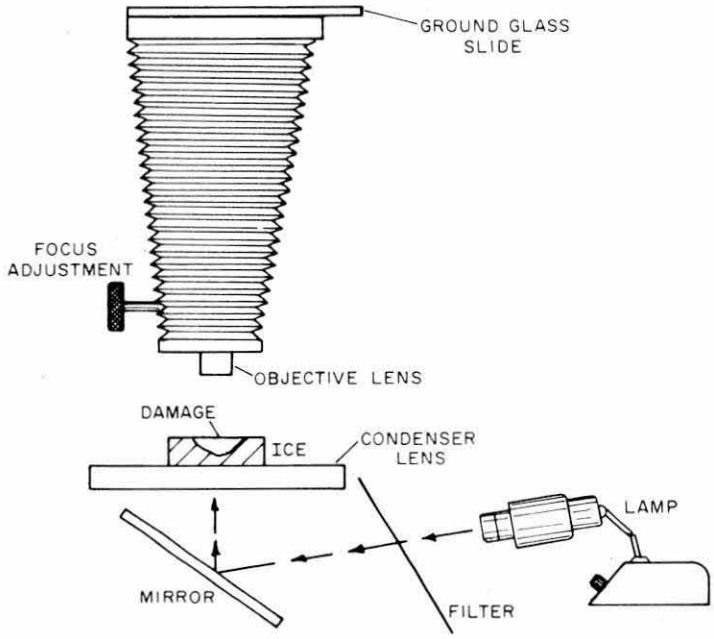

Figure 5. Photographic system for small-scale damage to the surface, method I.

Large cracks and fissures

If the damage was clearly visible without magnification, the photographic system shown in Figure 4 was used. The sample was illuminated obliquely with a 100-watt floodlamp. The camera was a Nikkon-F with a 55-mm Micro Nikkon lens having a 1:2 size ratio. The camera was mounted on a tripod and adjusted so that the damaged area of the sample filled the field of view. No alteration of the sample was necessary. The perspective from which photographs were taken was the direction of the laser's beam.

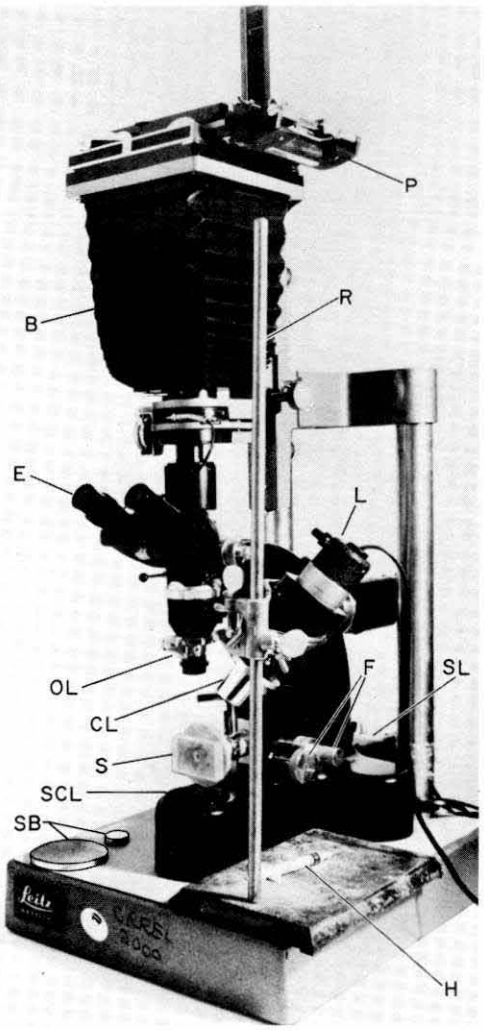

P Photographic plate holder

R Ring stand supporting illuminating lamp

B Bellows for camera

E Binocular eyepiece

L Illuminating lamp mounted to supply oblique, incident illumination to the sample

OL Objective lens

F Focusing controls

CL Condenser lens attached to illuminating lamp

SL Substage condenser lamp (not being used)

S Sample mounted on universal mount (see Fig. 7c)

SCL Well for substage condenser lens, which has been removed to allow use of universal mount

SB Substrate discs used in preparation of samples

H Hypodermic needle

Figure 6. Photographic system for small-scale damage to the surface, method II.

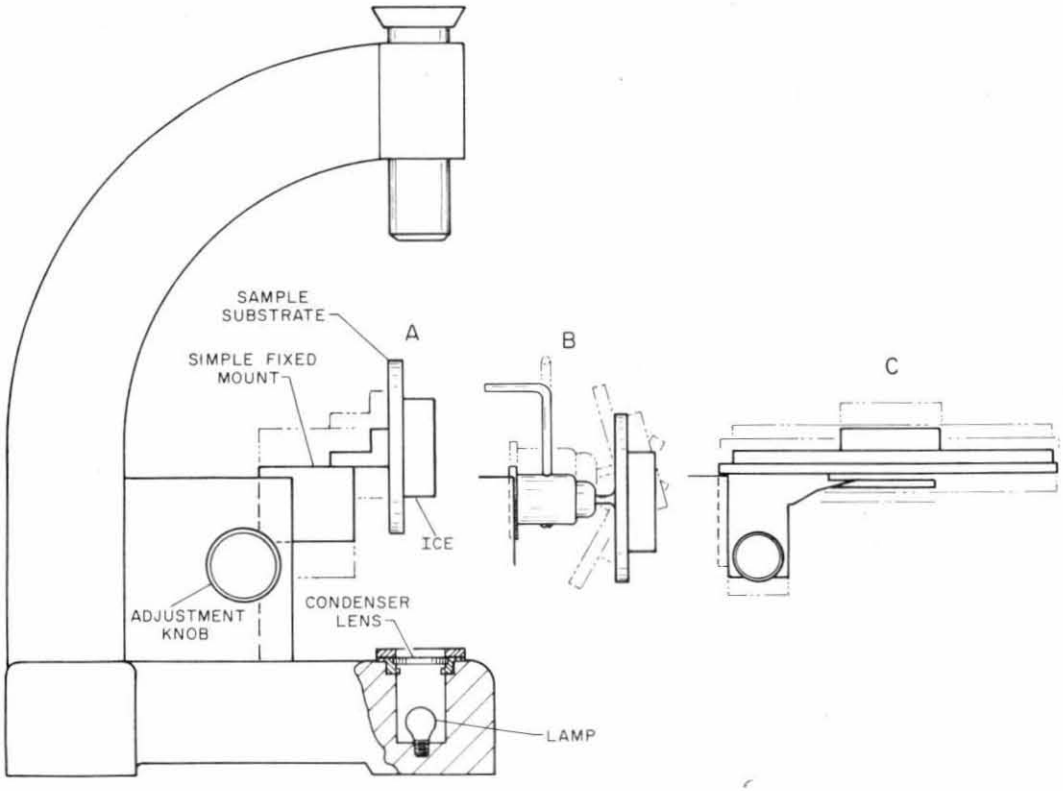

Figure 7. Options for mounting samples in photographic system. The microscope from the photographic system shown in Figure 6 can be fitted with: a) a simple fixed mount (fabricated from pieces of aluminum to provide the desired sample position), b) a universal mount that will allow 360 degree movement of the sample, or c) the fixed stage commonly found in microscopes used to work on thin sections.

Small damage to the surface

If the damage was localized at the surface and too small to be photographed directly, one of two methods was used. In both methods, photomacrographs were made with a Polaroid Land Film Holder no. 500 attached to a Leitz-Weitzler microscope; the magnification was of the order of 10X and the perspective was the direction of the laser's beam.

In the first method, the substrate was removed and the photographic system was in the configuration shown in Figure 5. This allowed the photomacrographs to be taken by transmission.

The second method was used if it was not feasible to remove the substrate. The photographic system was in the configuration shown in Figure 6, which allowed the photomacrographs to be taken by reflection.

Small damage to the bulk

If the damage was localized in the bulk of the ice and required magnification, one of two methods was used. Both methods made use of the same camera and the same microscope as the methods used for photographing small damage to the surface. The magnification was again of the order of 10X. Both methods allowed photomacrographs to be taken by transmission.

In the first method, the substrate was removed. The sample was further reduced in size to isolate the damaged volume without altering it. The resulting surfaces were smoothed so as to leave the

damage sandwiched between smooth, parallel surfaces suitable for use in the microscope. The system shown in Figure 5 was then used. The perspective from which photomacrographs could be taken was dictated by the configuration and extent of the superfluous ice that would have to be removed.

The second method was used when it was not feasible to remove the substrate. The photographic system was modified by the substitution of a universal joint (or simple aluminum mount) for the microscope's stage (Fig. 7). The sample (with the substrate still attached) was prepared by removing superfluous ice as in the first method. The modified stage made it possible to accommodate the substrate. The perspective from which photomacrographs could be taken was limited by the need to remove superfluous ice and the presence of the substrate. In particular, the latter limitation eliminated all perspectives but those from directions perpendicular to the laser's beam.

RESULTS

As no quantitative measure was available for characterizing the type and degree of damage, the standard data collection system described in Table I was used throughout the experimental work to provide a means of recording a qualitative description of the results of irradiation. When the key words defined in Table I are used, they are used in that context. The numerical code n assigned to a specific mode of damage was chosen in an attempt to award the largest number to the most severe damage. The concept of "most severe damage" was influenced by the objectives of this work, so damage considered most useful in the removal of ice from a substrate was judged as most severe.

The actual process of recording data on damage was as follows. As damage was observed, the key word and corresponding value of n which most nearly described the damage were recorded. Then, sketches of the damage site were made from two perspectives – from the direction of, and from a direction perpendicular to, the laser's beam. Any relevant comments as to special circumstances that accompanied the event that created the damage were recorded. If photographic work was possible, the sketches were augmented by photographs taken from one of the same two perspectives as the sketches.

The description of the results will be given in six subsections below. The first five subsections are primarily concerned with the results of the earliest experimental runs of which the objective was to determine the parameters that were most important. The sixth subsection presents systematic data in which the parameters to be investigated are those indicated by the early experiments. In the discussion of these six subsections, the numerical code for damage n will be extensively used. In addition, it will be useful to introduce the concept of "percentage cracking" p, which will be defined as

$$p = \frac{(\text{no. of irradiations of a specified type that yield } n > 2)\ 10^2}{(\text{total no. of irradiations of the specified type})} \qquad (2)$$

where "specified type" implies a set of restrictions on either the configuration of the optical system or the nature of the sample or a combination of both. The restrictions are chosen to suit the aspect that is to be studied.

Damage as a function of the position x of the focal point; $n(x)$

Three settings of x were studied – the surface of the ice, the center of the bulk of the ice, and the interface between the ice and the substrate. For brevity, these positions will be referred to as "surface," "bulk," and "interface," respectively.

Table I. Standard data collection system.
The numerical code n and the given definition were used to describe damage produced by the interaction of an optical beam with ice.

Key word	n	*Definition*
None	0	No discernible damage by visual inspection.
Discoloration	1	Visual inspection reveals a change in color but no discernible mechanical damage.
Pit	2	Visual inspection reveals mechanical damage having all dimensions approximately equal and not extending through the thickness of the ice and not appearing to involve any macroscopic removal of mass.
Crack	3	Visual inspection reveals mechanical damage having one dimension considerably larger than the others and not extending through the thickness of the ice and not appearing to involve any macroscopic removal of mass.
Fissure	4	Visual inspection reveals mechanical damage extending through the thickness of the ice but not appearing to involve any macroscopic removal of mass.
Chip	5	Visual inspection reveals mechanical damage involving macroscopic removal of mass but not extending through the thickness of the ice.
Hole	6	Visual inspection reveals mechanical damage involving macroscopic removal of mass and extending through the thickness of the ice.
Melting	7	Visual inspection reveals macroscopic disruption of the surface due to the formation of water that can not be attributed to condensation.

It was found that:

for CAG, CMS and UAG samples:

$$n(x = \text{surface}) = 1 \text{ or } 2; \quad n(x = \text{bulk}) = 0; \quad n(x = \text{interface}) = 2 \text{ to } 4 \tag{3}$$

and for SCR samples:

$$n(x = \text{surface}) = 2; \quad n(x = \text{bulk}) = 3; \quad n(x = \text{interface}) = 3 \text{ or } 4 \tag{4}$$

and for SI samples:

$$n(x = \text{surface}) = 5 \text{ to } 7; \quad n(x = \text{bulk}) = 0; \quad n(x = \text{interface}) = 0. \tag{5}$$

Relations 3, 4 and 5 make it clear that, for all samples other than SI, the optimum setting for x is the interface if the objective is to maximize damage. For SI samples, the optimum setting for x is the surface.

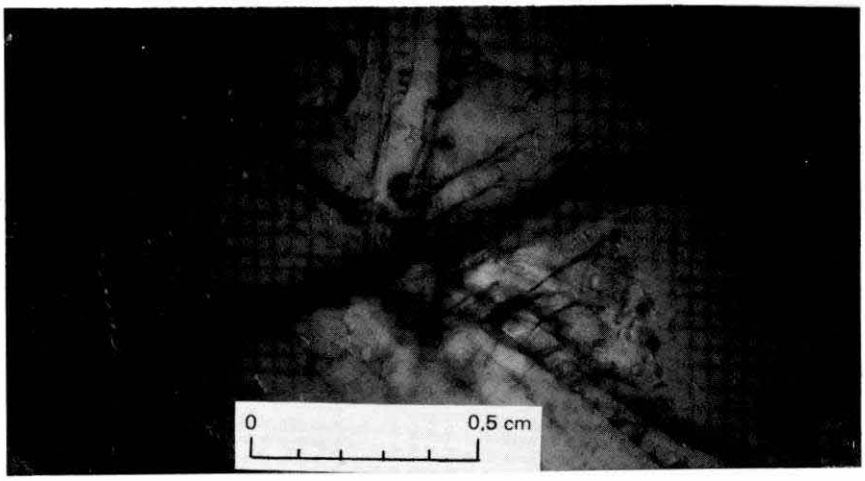

$\hat{c} = \parallel$

a. Optic axis parallel to the direction of irradiation.

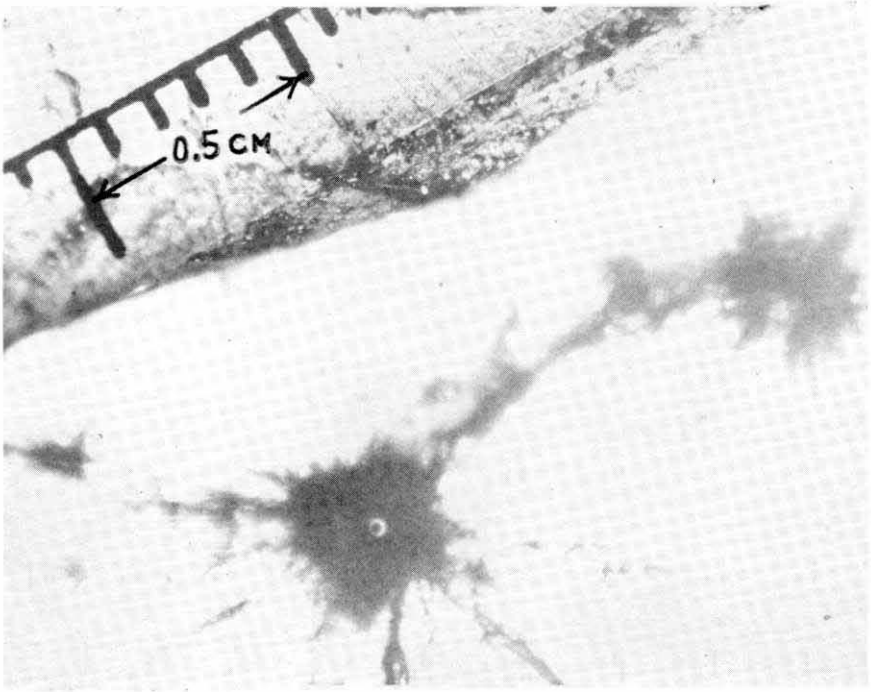

$\hat{c} = \perp$

b. Optic axis perpendicular to the direction of irradiation.

Figure 8. Typical fissures produced in SCR samples. Photographs taken in the direction of irradiation of SCR sample.

Damage as a function of the number of irradiations #; $n(\#)$

The value of # was varied from 1 to 15 for the same position of the same sample and this procedure was repeated for a variety of samples and optical configurations. It was found that, if damage occurred, it was produced by the first irradiation and the subsequent irradiations neither extended the damage nor introduced new damage. Repetitive irradiation of the same position with the same optical configuration was therefore ineffective in propagating damage. Therefore, the optimum value of # is unity.

Damage as a function of crystallographic orientation $\hat{c}$, $n(\hat{c})$; $p(\hat{c})$

The symbol $\hat{c}$ will represent a unit vector in the direction of the optic axis of a single crystal of ice. Three types of orientations were studied by use of the SCR samples – with $\hat{c}$ parallel to the laser's beam, with $\hat{c}$ perpendicular to the laser's beam, and with $\hat{c}$ neither parallel nor perpendicular to the laser's beam. For brevity, these three orientations will be indicated as $\parallel$, $\perp$ and *not*.

It was found that p was greater for $\hat{c} = \parallel$ than for $\hat{c} = \perp$ and that p was zero for $\hat{c} = not$. The maximum value of n that was observed was 4 for both of the orientations for which damage was observed. The configuration of the cracks and fissures that were produced was distinctive for a given orientation. This result is shown in Figure 8, which shows photographs of fissures observed in SCR samples. It can be seen that for $\hat{c} = \parallel$, the fissure consists of six lateral cracks intersecting (at the point where the beam entered the sample) at nearly equal angles (Fig. 8a). For $\hat{c} = \perp$, the fissure consists of four lateral cracks intersecting at unequal angles (Fig. 8b). In the former orientation, the damage usually consisted of exactly six intersecting cracks. In the latter orientation, the number of intersecting cracks varied but was never more than four and, usually, at least two cracks intersected at 90°.

Damage as a function of surface structure

The five types of samples could be ordered with respect to the relative smoothness of their surfaces. Such an ordering would give UAG, CAG, SI, CMS and SCR in the direction of increasing smoothness and would span the range from a surface like that on a natural accretion of ice (UAG) to an optically flat surface (SCR). Surface smoothness could be expected to influence the optical interaction with the ice because the electric field of the irradiating beam is known to interact strongly at projections on a rough surface, thereby dissipating energy and concentrating any damage upon the surface.[9]

Since the objective was to damage ice enough to aid in its removal from the substrate, the question to be answered was whether a naturally grown surface of ice would be too rough to allow more than ineffectual surface damage to be produced. Therefore, p was calculated for each type of sample with the restriction that the position of the focal point be the interface. In order of increasing smoothness, the values of p were 25, 12, 20, 20 and 35%, which implies that it is almost as easy to produce cracks in the bulk of a UAG sample as in an SCR sample.* It was concluded that naturally grown surfaces of ice would not be sufficiently rough to render the optical method of introducing damage infeasible.

Damage as a function of age A; $n(A)$

As ice accumulates upon a substrate, it may incorporate internal strains due to air bubbles, impurities, and interaction with the substrate. As the ice ages, some of these strains could relax through the action of the ordinary processes of the microstructure of the ice. Such phenomena have been observed before in ice[21] and were observed but not studied in these experiments.

In these experiments, A averaged 0.25 day, varied between 0.16 and 1.25 days, and was less than 0.5 day for the most reliable data. Since both the literature[21] and first-hand observations indicated that a time period of more than 0.5 day is needed to observe aging effects, it was thought that the available data did not warrant any conclusions as to the possible effects of aging.

---

* These values of p indicate that CAG samples are about three times more difficult to damage than the other four types of samples. This apparent difference may be due to the nonuniform distribution of bubbles in CAG samples as compared to other types or to the fact that the flexible mold in which CAG samples were grown served to relax internal strains during the freezing process. However, the data are insufficient to determine whether this apparent difference is real or a statistical artifact. For UAG, CAG, SI, CMS and SCR samples, the respective values of p were computed from the following populations of samples: 806 UAG samples, 17 CAG samples, 20 SI samples, 5 CMS samples, and 73 SCR samples.

Damage as a function of wavelength λ; $p(\lambda)$

Insufficient data were taken to allow the effects of wavelength to be rigorously separated from the effects of other parameters. However, p for each of the two wavelengths can be compared with p for all irradiations. The result is

$$p(\lambda = 6943\ \text{Å}) = 28\%; \qquad p(\lambda = 1.06 \text{ micrometers}) = 20\%; \qquad p(\text{all}) = 22\% \tag{6}$$

which implies that no significant difference in the probability of producing cracks was observed. However, such a conclusion is premature until additional experiments are performed both because of the possible masking influences of other parameters and because it is well-known that ice exhibits stronger absorption of light at 1.06 micrometers than at 6943 Å.[10]

Systematic study of damage as a function of W, t, m and s; $n(W, t, m, s)$

Experience gleaned from the experiments described above led to the narrowing of the list of parameters to be studied in detail to energy density W, thickness t, mode of operation of the laser m, type of substrate s, age, and focal length of the converging lens. This list was further shortened by the deletion of age and focal length, which it was decided should be studied in future experiments. In performing work to study $n(W, t, m, s)$, it was decided to use only UAG samples, set x = interface, $\# = 1$, $A = 0.25 \pm 0.05$ day, and $\lambda = 1.06$ micrometers; and to perform at least three runs for each setting of W, t, m and s. This was done and the results are given in Table II.

The description of the laser in the discussion of experimental procedure makes it clear that m and W are not strictly independent variables. In general, the lowest value of W obtainable for $m = N$ (normal mode) is larger than the highest value of W obtainable for $m = Q$ (Q-switched mode). Also, difficulties in controlling the value of W for a specific setting of m made it impossible to secure enough data to separate variables rigorously. With these reservations, the data in Table II appear to suggest the following conclusions:

1. The energy density at which ice first shows visible damage is from 4 to 8 times greater for $m = N$ than for $m = Q$ and this is true for all the thicknesses and substrates observed.

2. The energy density at which ice first shows visible damage increases with increasing thickness for all substrates and both modes of operation of the laser.

3. There is no conclusive evidence that the energy density at which damage is first observed depends upon substrate but the data suggest that any such dependence will be different for the two modes of operation of the laser and may also be strongly dependent upon thickness (of the ice) for some substrates.

4. For all substrates except concrete, the increase in damage for an increase in energy density at a given thickness is largest for $m = Q$. For concrete, the reverse is true. The change in damage due to a change in energy density tends to increase as the substrate is changed from stone to concrete to brass to aluminum for $m = Q$. The behavior for steel and asphalt is too dependent upon thickness to display any consistent ranking of these substrates relative to the others. For $m = N$, the increase is for a change of substrate from aluminum to stone to steel to concrete with brass and asphalt behaving essentially like aluminum. This indicates again that any dependence of the relationship between damage and energy density upon substrate may be different for different modes of operation and thicknesses.

5. For both modes of operation of the laser and all substrates and energy densities, the degree of damage either decreases or remains the same as the thickness is increased; the amount of change in damage with a change in thickness is greater for $m = N$ than for $m = Q$.

Table II. Experimental results from the study of $n(W, t, m, s)$. Conditions: x = interface, # = 1, A = 0.25 ± 0.05 day, λ = 1.06 micrometers. UAG samples. The focal length of the condensing lens was 10 cm.

m = N-mode

n	W (J/cm^2)	s
t = 0.5 cm		
0	37.2	Stone
0	57.3	
4	78.6	
4	104.4	
4	149.0	
0	44.6	Steel
3	49.0	
3	91.7	
3	143.2	
0	43.0	Concrete
0	50.0	
4	51.6	
4	94.5	
4	150.9	
4	156.3	
3	44.6	Brass
3	90.1	
3	140.7	
0	43.0	Aluminum
0	106.7	
3	136.2	
3	45.8	Asphalt
3	47.1	
4	51.6	
t = 1.0 cm		
1	40.1	Stone
3	93.3	
3	137.5	
3	151.8	
0	43.6	Steel
3	47.1	
3	88.8	
3	94.5	
3	46.15	Concrete
3	146.1	
4	154.7	
0	41.4	Brass
0	85.9	
1	89.1	
0	43.0	Aluminum
1	146.4	
0	43.0	Asphalt
0	45.8	

n	W (J/cm^2)	s
t = 1.0 cm (cont'd)		
3	49.0	Asphalt
3	82.75	
t = 1.5 cm		
0	17.2	Stone
0	46.15	
3	74.5	
0	48.7	Steel
2	51.6	
2	57.3	
2	98.7	
2	100.3	
3	145.8	
3	151.8	
0	36.0	Concrete
3	39.8	
3	74.5	
3	94.5	
3	126.0	
3	139.1	
0	40.1	Brass
0	60.5	
1	85.9	
2	95.8	
2	153.4	
0	33.4	Aluminum
0	175.1	
0	38.8	Asphalt
0	43.9	
3	77.7	
3	129.9	
t = 2.0 cm		
3	49.3	Stone
0	44.6	Steel
3	57.3	
0	43.0	Concrete
0	91.7	
3	141.6	
0	46.8	Brass
0	157.5	
0	43.0	Aluminum
0	154.7	
0	43.0	Asphalt
0	149.6	

Table II (cont'd).

m = Q-mode					
n	W (J/cm^2)	s	n	W (J/cm^2)	s
t = 0.5 cm			*t = 1.0 cm (cont'd)*		
4	12.4	Stone	0	10.0	Asphalt
4	15.9		3	12.9	
4	16.9		3	15.0	
4	22.0				
3	11.8	Steel	*t = 1.5 cm*		
3	12.4		0	5.4	Stone
4	14.3		0	23.55	
4	18.8		0	6.0	Steel
4	22.9		0	13.05	
3	6.0	Concrete	3	13.7	
4	12.4		3	24.8	
4	23.9		3	8.6	Concrete
3	8.4	Brass	3	17.8	
3	12.4		3	18.1	
4	12.7		0	2.5	Brass
4	17.5		0	18.5	
4	24.5		3	23.2	
3	7.95	Aluminum	3	25.1	
3	9.2		0	4.1	Aluminum
4	12.4		0	6.4	
4	21.5		2	7.95	
0	1.3	Asphalt	3	19.1	
3	11.8		0	12.1	Asphalt
4	13.05		0	12.7	
t = 1.0 cm			3	12.9	
3	8.6	Stone	3	23.1	
3	10.5		*t = 2.0 cm*		
3	12.4		0	7.95	Stone
3	24.2		0	24.8	
0	3.2	Steel	0	6.4	Steel
0	9.9		0	12.9	
2	12.4		3	13.0	
3	12.7		3	13.4	
3	18.5		3	17.8	
3	22.6		3	27.05	
0	8.6	Concrete	0	6.0	Concrete
3	12.7		0	14.6	
3	18.1		3	7.0	Brass
3	25.8		3	8.6	
0	11.1	Brass	3	13.05	
3	13.05		3	15.6	
0	10.2	Aluminum	0	6.7	Aluminum
3	12.4		0	12.7	
3	12.7		3	13.4	
3	16.9		0	7.0	Asphalt
3	23.2		0	22.9	
3	25.8		3	26.1	

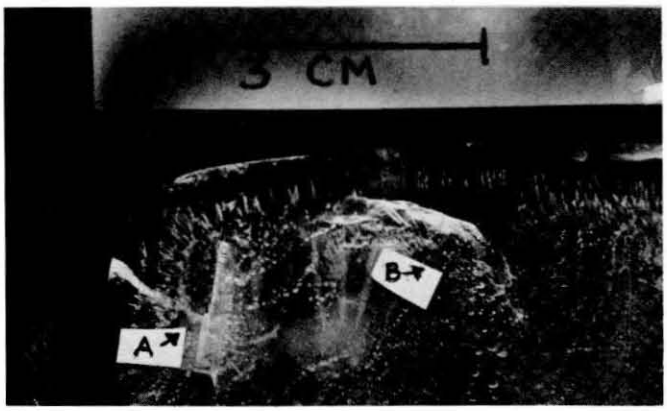

a.

$n_A(W,t,m,s) = 4(13.05\ J/cm^2,\ 0.5\ cm,\ Q,\ asphalt)$

$n_B(W,t,m,s) = 4(51.6\ J/cm^2,\ 0.5\ cm,\ N,\ asphalt)$

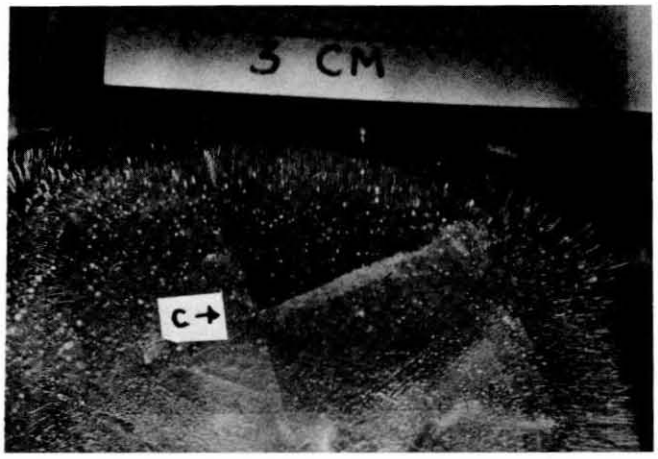

b.

$n_C(W,t,m,s) = 3(8.4\ J/cm^2,\ 0.5\ cm,\ Q,\ brass)$

Figure 9. Photographs representative of damage to UAG samples. The damage is described numerically in Table II. In a-f the direction of the optical beam that created the damage was perpendicular to the plane of the photograph. In g the direction of the optical beam is given by the arrowhead insert. All other inserts show point of impact of optical beam.

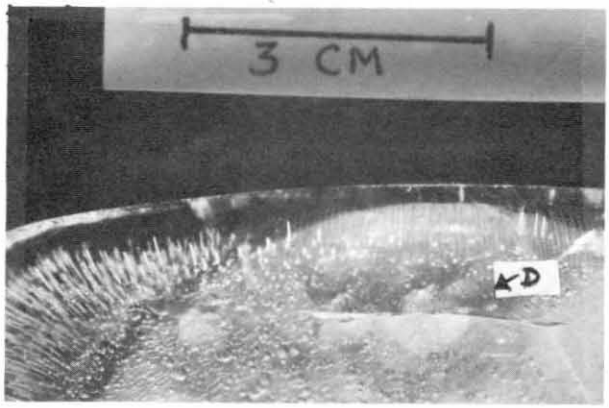

c.

$n_D(W,t,m,s) = 4(18.8\ J/cm^2,\ 0.5\ cm,\ Q,\ steel)$

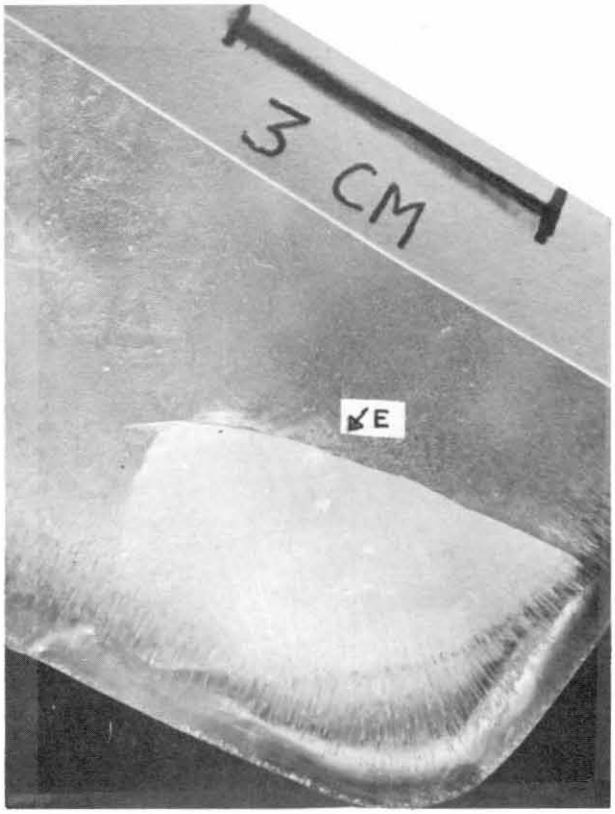

d.

$n_E(W,t,m,s) = 3(12.4\ J/cm^2,\ 1.0\ cm,\ Q,\ aluminum)$

Figure 9 (cont'd).

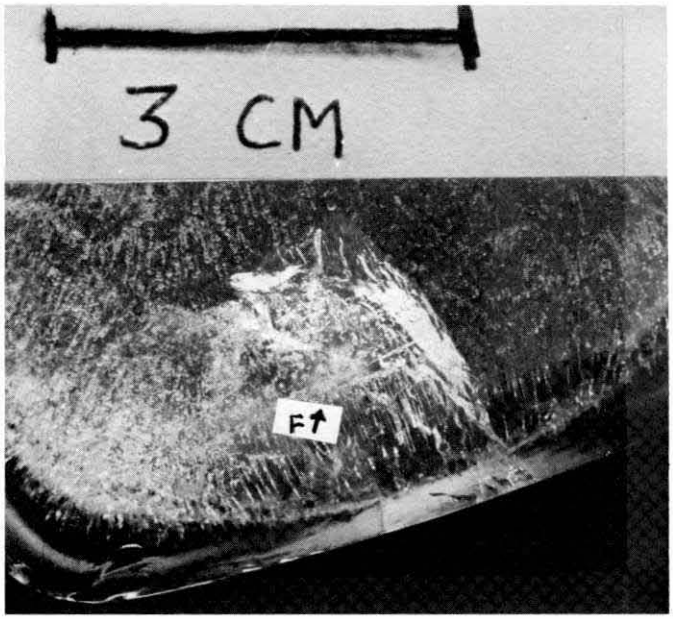

e.

$n_F(W,t,m,s) = 4(154.7\ J/cm^2,\ 1.0\ cm,\ N,\ concrete)$

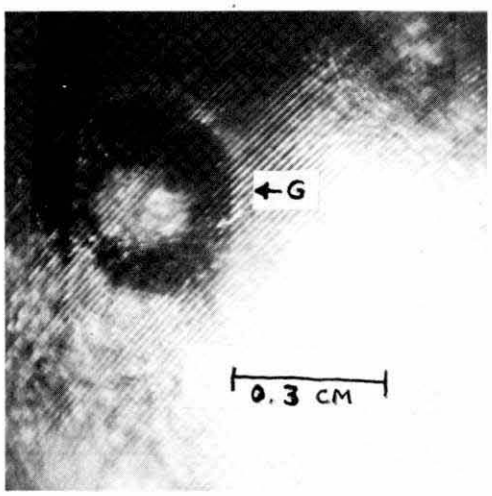

f.

$n_G(W,t,m,s) = 2(100.3\ J/cm^2,\ 1.5\ cm,\ N,\ steel)$

Figure 9 (cont'd). Photographs representative of damage to UAG samples. The damage is described numerically in Table II. In a-f the direction of the optical beam that created the damage was perpendicular to the plane of the photograph. In g the direction of the optical beam is given by the arrowhead insert. All other inserts show point of impact of optical beam.

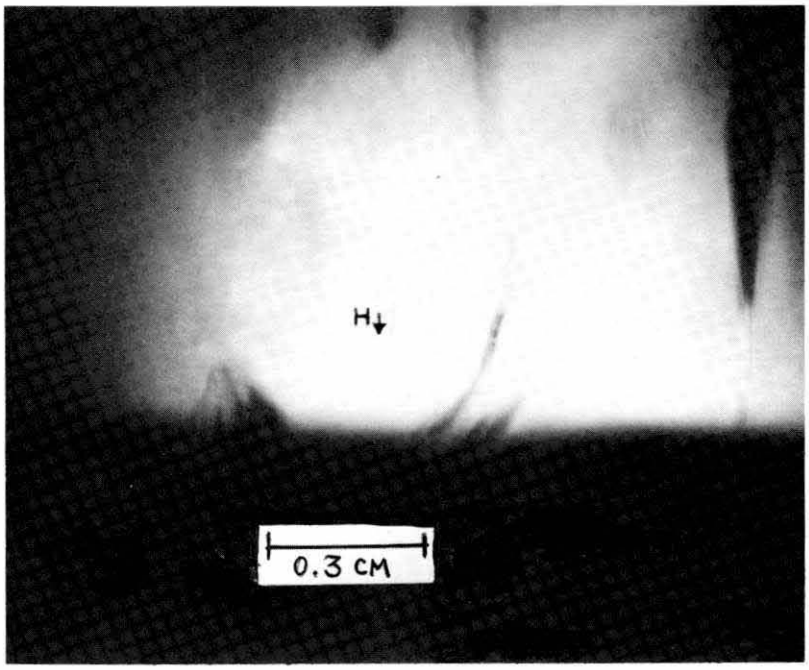

g.

$n_H(W,t,m,s) = 3(74.5\ J/cm^2,\ 1.5\ cm,\ N,\ concrete)$

Figure 9 (cont'd).

Although the data in Table II do not display any consistent differences between the behavior of ice grown on nonmetallic substrates and that grown upon metallic substrates, the appearance of the damage may be correlated with the metallic or nonmetallic character of the substrate. This is shown in Figure 9, which is a series of photographs representative of the data recorded in Table II. Figures 9a and e may be compared to Figures 9b-d. The former show damage in ice grown on nonmetallic substrates and the latter damage in ice grown on metallic substrates. It can be seen that the cracks and fissures are more irregular in structure for the nonmetallic substrates.

In Figure 9, all of the photographs except Figure 9g were taken with the camera aimed in the direction of the laser's beam. Figure 9g was taken with the camera aimed perpendicular to the laser's beam. Compare Figure 9g with Figure 9e; the curved, irregular outlines of the fissure in Figure 9e correspond to the traces in the top surface of a crack similar to that shown in Figure 9g. Note, in the crack in Figure 9g, the curved surfaces radiate from the focal spot at the interface so that the crack resembles a bowl sitting upon the interface. This type of structure was typical of cracks that were observed in nonmetallic substrates and was very seldom observed in metallic substrates. Cracks in ice grown on metallic substrates usually were flat surfaces perpendicular to the surfaces of the specimen and parallel to the laser's beam.

Figures 9f and g display what may be the stages of damage. That is, it may be that fissures are generated by the initial creation of a pit on the interface at the focal point. (Figure 9f shows such a pit.) Then, if conditions are favorable, the interaction of the initial damage with the rest of the ice may generate a small crack such as that shown in Figure 9g. This crack may develop further into a large crack or fissure that is visible at the top surface of the ice or which shatters the ice.

ANALYSIS

In this section, an attempt will be made to compare some of the implications of the observations reviewed in the preceding section with what is known about the physical properties of ice and the current speculations as to the mechanisms by which optical beams induce damage in transparent materials.

Fracture in ice

When a stress is applied to a crystalline solid, the solid may deform by the motion of characteristic systems of dislocations or "slip-systems." If the stress is sufficiently high, applied too rapidly, directed in a direction in which plastic deformation is difficult, or otherwise applied in such a manner that it cannot activate the available systems of dislocations, the solid may fail by fracture.

Ice as ordinarily encountered is characterized by a hexagonal unit cell containing four molecules. The oxygen atoms are arranged in the Wurzite structure but the hydrogen atoms are not in an ordered configuration.[15] This type of ice has two independent slip-systems. The first slip-system is slip on (0001)-planes by dislocations with Burger's vector $(a/3)<11\bar{2}0>$. The second is slip on $(10\bar{1}0)$- or $(10\bar{1}1)$-planes by dislocations with Burger's vector $(a/3)<11\bar{2}0>$.[11,27] In general, the first slip system is more easily activated than the second.

Experimental work has shown that when a compressive stress is applied to a polycrystalline sample of ice, any cracks that form lie in planes parallel to the direction of the stress and involve only one or two grains. A majority of such cracks are parallel or perpendicular to (0001). If the crack involved only one grain, the crack's edge was usually located at the boundary of the grain. If the crack involved more than one grain, the crack's edge changed direction at the boundary between the grains so that it remained either parallel or perpendicular to [0001] or else curved into the (0001)-plane and terminated. When a thermal shock was applied instead of the compressive stress, a pattern of cracks characteristic of relative grain orientation was observed – a triangular array of cracks parallel to $(10\bar{1}0)$ where [0001] was perpendicular to the surface, a rectangular array of cracks parallel to $(10\bar{1}0)$ or $(10\bar{1}1)$ where [0001] was parallel to the surface, and, for other orientations, an irregularly curved pattern of cracks. These observations are interpreted to imply that when stress is applied in an essentially two-dimensional manner, ice has only one independent slip-system available to respond, so many of the grains of a polycrystal can not maintain constant volume while deforming under the influence of the stress. Internal stresses are concentrated at grain boundaries. If the grains are oriented in such a manner that the deformation of a grain interferes with the deformation of the adjacent grains, any concentration of stresses at the grain boundary will be relieved by the formation of cracks instead of deformation. At a temperature of -20°C, ice is observed to fracture at tensile stresses of the order of 10^6 newtons/m^2.[27]

Mechanisms for optically generated damage in transparent dielectrics

The mechanisms that have been proposed to explain the production of damage (in transparent materials) by intense optical beams are 1) absorption of light at defects in the material, 2) stimulated Brillouin scattering, 3) multiphoton absorption, 4) intraband absorption, 5) generation of high temperatures due to the creation of microplasmas, and 6) superposition of stress waves.[23] The experimental work seems to indicate that no one of these mechanisms explains all the damage that is observed. Combinations of these mechanisms assisted by self-focusing of the optical beam may be the true explanation. It also seems likely that different mechanisms are operative in different materials.

Ice is known to exhibit Bjerrum defects (defects in the orientation of the hydrogen atoms such that the Bernal-Fowler rules are violated), ionic defects, and dislocations.[8] Since there are four

molecules per unit cell, it has at least 12 branches in its acoustic dispersion. The disorder of the hydrogen atoms could affect the interaction of the lattice with an optical beam and the hydrogen atoms themselves could interact with an optical beam. It is therefore possible that any or all of the mechanisms that were listed above could be effective in creating optical damage in ice.

Self-focusing of the optical beam by the material can be important in concentrating the intensity of the optical beam such that stresses high enough to produce damage are generated in a localized area. This phenomenon depends upon a change in refractive index produced by the electric field of the optical beam (Pockels and/or Kerr effects) and the distribution of the intensity of the electric field in the cross section of the optical beam. (Usually, this distribution is Gaussian for lasers.) Very little work on the effects of intense electric fields on ice has been done and it is not clear whether ice exhibits self-focusing to any significant degree. In discussing nonlinear optical interactions, it is customary to define a set of electrooptic coefficients by expanding the energy stored in a unit volume of a dielectric in powers of the applied electric field. The linear term of this power series has a third rank tensor as coefficient, the quadratic term has a fourth rank tensor as coefficient, and so forth. The linear term describes what is known as the Pockels effect and the quadratic term describes the Kerr effect.[16] The form that these two tensors assume depends upon the crystalline structure of the material they characterize. Ice belongs to one of the 11 crystal classes that possess a center of inversion[15] and therefore can not exhibit a Pockels effect as the relevant third rank tensor must vanish. However, the fourth rank tensor that describes the Kerr effect must have the five independent components T_{1111}, T_{1122}, T_{1133}, T_{3333} and T_{2323}.[16] This implies that at least some self-focusing should occur for a sufficiently intense optical beam traveling through ice. It also implies that such an effect should be dependent upon the orientation of the crystal relative to the direction of the optical beam.

For stimulated Brillouin scattering to be the sole mechanism for the damage in ice, pressures of the order of the threshold for tensile fractures (10^6 newtons/m^2 = 10^7 dynes/cm^2) or greater[27] would have to be generated by the electrostriction produced by the scattering. Under the experimental conditions in this work, the electric field at the focal point (assuming x = interface) in the ice would be approximately 1.7×10^3 statvolts/cm for an optical pulse delivering a power density of 4.45×10^{15} erg/cm^2 sec. An estimate of the relationship between the stiffness C, the electrostriction G, the electric field E, and the pressure p_e generated by G is (for CGS units)[23]

$$p_e = CE^2G. \tag{7}$$

This implies that, for the conditions of these experiments, G would have to be of the order of 3×10^{-11} cm^2/statvolt^2 if C is taken as 1.2×10^{11} dynes/cm^2.[11] This value for G is two orders of magnitude higher than that for glass[23] so it is doubtful that stimulated Brillouin scattering alone could account for the observed damage. However, if self-focusing effects are significant in ice, it would be possible for the electric field to be enhanced so that it would be much greater than that assumed in the calculation above.

Until more is known about the relevant properties of ice, such as the size of the dynamic fracture stress or the electrostriction, it is not possible to distinguish quantitatively between the possible mechanisms for damage.

Discussion of the results

The results for damage as a function of position of the focal point may be compared with results in the literature for polymethyl methacrylate and glass.[23] These results showed that the size of the damaged area increased as the focal point was moved toward the rear of the sample, reached a limiting value in the bulk, maintained this value until the rear surface was reached, and decreased as the

focal point passed out of the sample. The samples were all free-standing, that is, not attached to a substrate as for the samples in the experiments reported here. The fact that for free-standing samples damage did not increase at the rear surface, while for samples that included substrates the damage increased with distance into the sample and reached a maximum at the interface indicates first that the confinement of the beam in the bulk increases damage and second that the process of reflection and absorption of the beam by the substrate acts to further increase the damage. Thus, ice adhering to a substrate is more easily damaged than free-standing ice.

Since the SI samples were not transparent, the structure of the bulk acted to scatter the beam and dissipate rather than concentrate the optical energy unless the beam was focused at the front surface.

The fact that the optimum value of # was found to be unity agrees with results reported for alkali halides[22] but cumulative effects have been observed for polymethyl methacrylate.[23]

The results observed for SCR samples correspond with the crystallography of ice and the fact that differing patterns of cracks were observed for different orientations of the optic axis agrees with the data for the fracture of ice that were discussed above. The fact that despite some dissipation and scattering of the beam by rough surfaces and air bubbles, UAG samples were almost as easily damaged as SCR samples indicates that the damage in the UAG samples may be interpreted in terms of stress concentrations at boundaries between grains in incompatible orientations as explained in the discussion of fracture.

In general, results reported in the literature for other transparent materials agree with the result that operation of the laser in the normal mode is less effective in producing damage at a given energy density.[5 19] The essential difference between operation in the two modes is the power delivered by the resulting pulse. Therefore, an increase in power density is more effective in increasing damage than increasing the energy density without increasing the power density. This suggests that the more powerful pulse generated for $m = Q$, even though it is lower in total energy, applies a stress to the sample too rapidly for the normal mechanisms of stress relief to operate and therefore induces local failure of the material by fracture.

The decrease in damage as the thickness of the ice is increased (observed for UAG samples) can be understood in terms of the increase in scattering centers such as air bubbles that must occur as a UAG sample becomes thicker. These scattering centers effectively decrease the transparency of the sample and partially defocus the beam so that the actual energy density delivered to the interface is less than that calculated from eq 1.

The substrate can affect the degree of damage in several ways. The smoothness of the substrate's surface can affect the nucleation of the ice in the early stages of growth. The strength of the adhesion between substrate and ice is a function of the state of the substrate's surface, the surface energies of ice and the substrate, the temperature during growth of the ice, and a variety of other parameters.[2 14] The thermal coefficient of expansion B is different for ice and the substrate and so it is possible for the resulting differential rates of contraction during freezing to produce strains in the ice that would act as concentrators of internal stress and preferential sites for damage when irradiated. If ΔB is defined for a given sample as

$$\Delta B = B(\text{substrate}) - B(\text{ice}) \tag{8}$$

damage due to this effect would be largest for the sample with the largest value of ΔB. If the substrate was a single crystal, then the periodic potential of its lattice at the interface could produce epitaxial effects in the ice.[24] Already mentioned is the fact that the substrate can heat the ice at the interface by absorbing the beam or else further concentrate the beam in the ice by reflecting the beam back upon itself. Therefore, the optical properties of the substrate could play a role in the interaction that produces the damage to the sample.

Table III. Thermal coefficient of expansion B for ice and various substrates.

Material	B $(^{\circ}C^{-1})$	*Source*
Aluminum 6061-T6	23.6×10^{-6}	*Aeronautical Vest Pocket Handbook,*
Steel A1S1 101E-1020	11.7×10^{-6}	Pratt and Whitney Aircraft, United Air-
Brass (free machining)	20.3×10^{-6}	craft Corporation, 9th ed., 1959.
Stone (granite)	7.2×10^{-6}	*Standard Handbook for Mechanical*
Stone (sandstone)	9.9×10^{-6}	*Engineers,* Baumeister and Marks,
Concrete	14×10^{-6}	7th ed., McGraw-Hill, 1967.
Ice	50.9×10^{-6}	

For the samples that were studied in this work, it is clear that the substrate's interaction with the beam does have some effect. The different results for the structure of the cracks formed in ice that was grown upon metallic as opposed to nonmetallic substrates can be explained by the differences in smoothness and optical properties of these two categories of substrate. That is, all of the nonmetallic substrates had rough surfaces compared to the metallic substrates and the latter were better reflectors of optical radiation. It is not clear whether any effect due to the differences in ΔB was observed. Table III gives approximate values of B for ice and five of the substrates that were used. The data for which the effects of the substrate could be studied indicate that a larger value of ΔB is not necessarily associated with more damage. It is possible that effects such as reflection and absorption of the beam mask the effect of differential rates of contraction. However, probably no additional internal stresses were generated in the UAG samples. This is because the values of ΔB for the UAG samples could be expected to generate stresses in excess of 10^6 newtons/m^2 and therefore lead to fracture of the sample's ice during freezing. Large cracks and fissures in the ice of UAG samples were observed before irradiation and areas of the sample that were not marred by these aberrations were chosen for irradiation. Therefore, the stresses generated by differential rates of contraction were probably relieved by fracture before the sample was irradiated, leaving the portion of the sample that was irradiated free of this type of internal stress.

Comparison of the structures of large and small damage suggests that the damage may begin as a pit at the interface created by the production of a high temperature at the focal point and consequent vaporization of a portion of the ice. As the expanding vapor would then be confined in the bulk of the sample, it could generate additional stress and propagate the damage in the most favorable crystallographic directions leading to the formation of large damage about the original pit.

SUMMARY AND CONCLUSIONS

The results indicate that it is feasible to fracture accumulations of ice on a surface by irradiation with a single optical pulse of energy 1 to 5 joules at a wavelength of 1.06 micrometers if the pulse is focused to a point of diameter less than 0.2 cm at the interface between the ice and the substrate. This can be accomplished with lasers of commercial design and inexpensive glass lenses.

The method is limited by the thickness of the ice; the thickness should be less than 2 cm for a laser operated in the Q-switched mode and less than 1.5 cm for operation in the normal mode. The

Q-switched mode of operation is more efficient in producing fracture. The type of substrate is not significant in the production of fracture but may be important in facilitating final removal of the ice from the substrate after fracture as a rougher surface may make it more difficult to remove the ice by fracture of successive segments. The size of the fracture that can be obtained with a single pulse is of the order of a few centimeters in cross section for ice of the order of 1 cm thick. Careful focusing of the pulse is the most critical element in the procedure. Allowances must be made for the wavelength of the light and the refractive index of ice in adjustment of the position of the focusing lens.

Data for optically induced damage to transparent materials other than ice indicate that the degree of damage may depend upon the focal length of the lens[23] and this should be investigated along with any possible dependence upon wavelength of the light and the age of the ice.

LITERATURE CITED

1. Borisenkov, E.P. et al. (1972) Investigation of the physical nature of ship icing. *Issledovanie Fizicheskoi Prirody Obledeniia Sudov*, Leningrad. USA CRREL Draft Translation 411, 1974.
2. Camp, P.R. and C.F. Barter (1965) Rate of growth of ice at an aluminum-water interface. *Nature*, vol. 206, p. 495.
3. Chang, D.B., J.E. Drummond and R.B. Hall (1970) High-power laser radiation interaction with quartz. *Journal of Applied Physics*, vol. 41, p. 4851.
4. Clark, A.F., J.C. Moulder and R.P. Reed (1973) Ability of a CO_2 laser to assist ice breakers. *Applied Optics*, vol. 12, p. 1103.
5. Cullom, J.H. and R.W. Waynant (1964) *Applied Optics*, vol. 3, p. 989.
6. DeWit, R. (1971) Relation between dislocations and disclinations. *Journal of Applied Physics*, vol. 42, p. 3304.
7. Dobbs, H.S., J.E. Field and A.H. Maitland (1973) Fracture surface energies using laser-induced cracks. *Phil. Mag.*, vol. 28, p. 33.
8. Eisenberg, D. and W. Kauzmann (1969) *The structure and properties of water*. New York and Oxford: Oxford University Press.
9. Fradin, D.W. and Bass, M. (1973) Comparison of laser-induced surface and bulk damage. *Appl. Phys. Lett.*, vol. 22, p. 157.
10. Glen, J.W. (1974) The physics of ice. USA CRREL Monograph II-C2a.
11. Glen, J.W. (1975) The mechanics of ice. USA CRREL Monograph II-C2b.
12. Goetze, C.G. (1965) A study of brittle fracture as applied to ice. USA CRREL Technical Note 90 (unpublished).
13. Itagaki, K. (1975) U.S. Army Cold Regions Research and Engineering Laboratory internal correspondence. Essentially, the geometry of crystalline growths on the crystals (hoarfrost) is observed and the orientation of the crystal deduced from this.
14. Jellinek, H.H.G. (1957) Tensile strength properties of ice adhering to stainless steel. U.S. Army Snow, Ice and Permafrost Research Establishment (USA SIPRE) Research Report 23.
15. Kamb, B. (1973) Crystallography of ice. *Physics and Chemistry of Ice* (E. Whalley, S.J. Jones and L.W. Gold, Eds.), Royal Society of Canada, Ottawa.
16. Kaminow, I.P. (1974) *An introduction to electrooptic devices*. New York and London: Academic Press.
17. Lane, J.W. (1974) Proposal for an investigation into use of high-energy lasers as de-icing units. U.S. Army Cold Regions Research and Engineering Laboratory internal correspondence (unpublished).
18. Marshall, S.J. (In prep.) Photomacrography of artifacts in transparent materials. U.S. Army Cold Regions Research and Engineering Laboratory, CRREL Report.
19. Martinelli, J. (1966) Laser-induced damage thresholds for various glasses. *Journal of Applied Physics*, vol. 37, p. 1939.
20. Milam, D., R.A. Bradbury and M. Bass (1973) Laser damage threshold for dielectric coatings as determined by inclusions. *Appl. Phys. Lett.*, vol. 23, p. 654.
21. Oguro, M. and A. Higashi (1973) Stacking-fault images in NH_3-doped ice crystals revealed by X-ray diffraction topography. *Physics and Chemistry of Ice* (E. Whalley, S.J. Jones and L.W. Gold, Eds.), Royal Society of Canada, Ottawa.
22. Olness, D. (1968) Laser-induced breakdown in transparent dielectrics. *Journal of Applied Physics*, vol. 39, p. 6.
23. Ready, J.F. (1971) *Effects of high-power laser radiation*. New York and London: Academic Press.
24. Shimaoka, G. and J.W. Lane (1967) The structure of copper thin films evaporated in an ultra-high vacuum. *14th National Symposium of the American Vacuum Society, 24-27 October 1967, Kansas City, Missouri* (W.J. Lange, Ed.), Herbick and Held Printing Co.
25. Smith, E. (1974) Effect of the discreteness of the atomic structure on cleavage crack extension in brittle crystalline materials. *Journal of Applied Physics*, vol. 45, p. 2037.
26. Tobin, T.M. and K. Itagaki (1970) A technique for producing strain-free flat surfaces on single crystals of ice. *J. Glac.*, vol. 9, p. 385.
27. Weeks, W.F. and A. Assur (1969) Fracture of lake and sea ice. USA CRREL Research Report 269.